ORIGINAL ARTICLE

Graphene nanoplatelets/CeO$_2$ nanotiles nanocomposites as effective antibacterial material for multiple drug-resistant bacteria

Saliha ur Rehman[1] · Robina Khan Niazi[2] · M. Zulqurnain[3] · Qaisar Mansoor[5] · Javed Iqbal[6] · Aqsa Arshad[1,4]

Abstract

Antibacterial agents with low toxicity to normal cells, redox activity and free radical scavenging property are urgently needed to address the global health crisis. The phenomenal conducting nature of graphene is a best fit to enhance the antibacterial properties of metal oxides. In this work, CeO$_2$ nanotiles and graphene nanoplatelets/CeO$_2$ nanotiles nanocomposites (G/CeO$_2$) have been synthesized by a solvothermal method. The prepared materials have been characterized using XRD, FE-SEM, EDX, and UV–visible spectroscopy techniques to investigate their crystallinity, morphology, composition, and optical bandgap energies. The CeO$_2$ and G/CeO$_2$ nanocomposites have also been tested for antibacterial applications. The neat CeO$_2$ nanotiles sample inhibits the bacterial growth of *Pseudomonas aeruginosa* and *Staphylococcus aureus* up to 14.21% and 39.53% respectively. The antibacterial activity was tremendously enhanced using 25% graphene-loaded sample (G/CeO$_2$-II) i.e., approximately 83% loss of *P. aeruginosa* and 89% in case of *S. aureus* has been observed. This can be attributed to the unique nano-architecture, oxidative stress due to the excellent ability of reversible conversion between the two electronic states of CeO$_2$ and the stress exerted by the planar graphene and CeO$_2$ nanotiles. Therefore, the G/CeO$_2$ nanocomposites can find potential application as nano-antibiotics for controlling pathogens.

Keywords Ceria nanotiles · Graphene nanoplatelets · Antibacterial properties

Introduction

Antimicrobial drug resistance (ADR) is one of the greatest health issues faced globally (Majumder et al. 2020). Antibiotics are the human defence armours that fight against pathogens, but the excessive use of antibiotics and rapid transfer of resistance genes has led to ineffective antibiotics. The alarming rate of worldwide antibiotic resistance has threatened the human health by increasing the mortality rate along with an increased treatment cost (AlSheikh et al. 2020). UN Ad hoc integrity coordinating group of antimicrobial resistance reported that drug resistance-related diseases cause 10 million deaths each year by 2025. Currently, 700,000 people die every year due to drug-resistant diseases, which includes 230,000 deaths due to multidrug-resistant (MDR) tuberculosis (TB). The severity of microbial co-infection is also highlighted in COVID-19 pandemic. Bacterial pathogens are highly probable to be found in viral respiratory infections like COVID-19. The use of antibiotics is essential in such cases (Langford et al. 2020). Therefore, the current global pandemic along with possibility of multiple drug resistance in the human body has posed major health challenges. TB, MRSA and VRE infections, diarrhoea, severe sexual complications and some CRE infections are caused by mycobacterium, *Vancomycin-resistant Enterococci*, Methicillin-resistant *Staphylococcus aureus* (MRSA), *Neisseria gonorrhoea*, *Clostridium difficile* and *Carbapenem-resistant Enterobacteriaceae*, i.e., *Klebsiella species* and *Escherichia*

✉ Aqsa Arshad
   aqsa.arshad@iiu.edu.pk

1 Department of Physics, International Islamic University, Islamabad, Pakistan

2 Department of Biological Sciences, International Islamic University, Islamabad, Pakistan

3 Department of Physics, The University of Cambridge, 9 JJ Thomson Avenue, Cambridge CB3 0FA, UK

4 Electrical Engineering Division, University of Cambridge, Cambridge CB3 0FA, UK

5 Institute of Biomedical and Genetic Engineering (IBGE), Islamabad, Pakistan

6 Laboratory of Nanoscience and Technology (LNT), Department of Physics, Quaid I Azam University, Islamabad, Pakistan

coli respectively. These bacteria have developed resistance to antibacterial drugs over the years. In many parts of the world, the high resistance of *E. coli* against fluoroquinolone antibiotics has made it ineffective in half of the patients suffering with urinary tract infections. The *Staphylococcus aureus* has also been resistant to first-line drugs. People with MRSA are 64% more probable to die than people with non-resistant form of bacteria (AL-Saadi 2016; Hibbitts et al. 2019). Therefore, some immediate steps are needed to prevent a potentially disastrous drug resistance, e.g., it is necessary to develop novel nano-medicines that have tendency to fight against bacterial infection-related morbidity.

Metal oxides have been a promising candidate (He et al. 2015) for the development of novel nano-antibiotics. They have other potential applications like photocatalysis, super-conductivity, electronics, nanorobotics, and automobile industry (Zhang et al. 2020; Huang and Chen 2009; Kim et al. 2010; Halder and Sun 2019; Meixner et al. 1995; Kummer 1986). Many transition metal oxides show significant antibacterial performance towards a wide range of Gram-negative and Gram-positive bacteria (Paul et al. 2020; Talat et al. 2020). These properties are further enhanced if the same materials with reduced dimensions are employed, which mainly is attributed to distinct physicochemical properties appearing at nanoscale (Sanpo et al. 2013; Wang et al. 2010). Metal oxides have a common feature of producing oxidative stress due to generation of reactive oxygen species (ROS) in presence of UV light. CeO_2 is unique as it can generate ROS even without UV light exposure (Jones et al. 2008). Moreover, the oxidative stress generation is a unique property of nano-CeO_2 because it has an excellent ability of reversible conversion between its two electronic states in an auto-regenerative cycle ($Ce^{4+} \rightarrow Ce^{3+} \rightarrow Ce^{4+}$) (Stoianov et al. 2014). CeO_2 being a natural scavenger of ROS and nitrogen species, oxidizes from Ce (III) to Ce (IV) in the presence of ROS and then undergoes back to Ce (III) through a regeneration process. Therefore, CeO_2 NPs can reduce oxidative stress by acting as antioxidants and may also be toxic to cancerous and bacterial cells by generating ROS under some conditions (Zhang et al. 2019). The ROS generating capability of CeO_2 contributes towards inhibition of the bacterial growth, which is due to the oxidative stress on lipids and proteins (that are found in plasma membrane of microorganisms) caused by the reduction of Ce (IV) into Ce (III) (Gliga et al. 2017). Therefore, the antibacterial properties of CeO_2 based materials are expected to be extraordinary as compared to other metal oxides, based on its naturally free radical scavenging property.

Also, metal oxide nanostructures with higher surface area than their bulk counterparts lead to higher chemical and biological activity. With these characteristics, metal oxide nanostructures can efficiently target cell membranes for better inactivation of bacteria (Subbiahdoss et al. 2012).

These properties are also expected to enable nano-CeO_2 to uniquely take up antibiotic drug resistance. However, it is always needed to add highly efficient antibiotic materials to the existing ones to combat ever increasing drug resistance (Bellio et al. 1860). Therefore, new strategies are required to improve antibacterial efficiency of CeO_2. Some methods include its modification using dopants and (or) by compositing it with other chemical species. An effective strategy can be the formation of its composites with graphene family nano-materials. Graphene and CeO_2 nano-composites have found various applications, e.g., as biosensors (Yang et al. 2016), cholesterol detectors (Zhang et al. 2013), catalysts (Yang et al. 2017), super-capacitive electrodes (Xie et al. 2018), anodes in lithium ion battery (Wang et al. 2011) and microwave absorbers (Wu et al. 2020).

Graphene-based metal oxide nano-composites have emerged as an extremely promising class of antibacterial materials due to their distinct electrical properties and low toxicity towards mammalian cells (Joung et al. 2011; Rojas-Andrade et al. 2017; Mathew et al. 2020; Alhazmi et al. 2022). When compared to published reports on biomedical applications of CeO_2, very limited information is available on the biomedical applications of graphene-based CeO_2 nanocomposites. Some related materials have been studied, e.g., antimicrobial efficiency of CeO_2/GO nano-composites has been tested (Kashinath et al. 2019; Bharathi and Stalin 2019). However, the anti-bacterial activity of CeO_2 and neat graphene nanocomposites has not been studied so far. Graphene-based composites are phenomenally effective in bacterial killing due to their bio-compatibility, sharp edges-based sheets like morphology and high specific surface area (Ni et al. 2010). Therefore, it can be anticipated that the antibacterial potential of CeO_2 may possibly be enhanced by the formation of a unique nano-architecture of G/CeO_2 nanocomposites.

Keeping in view the mentioned discussion, we aim to boost the antibacterial performance by synthesizing cutter-like morphology of CeO_2 nanostructures so that it can act synergistically with the sharp edges of graphene to achieve an outstanding bactericidal or bacteriostatic behaviour against both Gram-negative and Gram-positive bacteria. Therefore, in this work, we present synthesis of CeO_2 nano-tiles and G/CeO_2 nanocomposites and study their structural, morphological, optical, and antibacterial properties against two model pathogenic bacterial strains *S. aureus* and *P. aeruginosa*. *S. aureus* is found in skin and respiratory tract, causes a wide range of clinical infections i.e., pneumonia, pimples etc. It is a Gram-positive bacterium (Tong et al. 2015). *P. aeruginosa* causes pneumonia, septic shock and many blood infections in humans (Todar 2006). To the best of our knowledge, this is the first report on the synthesis of CeO_2 nanotiles and the investigation of antibacterial behaviour of G/CeO_2 nanocomposites.

Experimental

Preparation of CeO$_2$ nanotiles

The materials used for making CeO$_2$ and G/CeO$_2$ nanocomposites are: cerium nitrate hexahydrate Ce(NO$_3$)$_3$.6H$_2$O, 5 M aqueous sodium hydroxide solution (NaOH), isopropyl alcohol (99%, Sigma Aldrich), ethyl alcohol (99%, Merck), citric acid (C$_6$H$_8$O$_7$), distilled water and graphene nanoplatelets (100%, KNANO) with the thickness ≤ 15 nm and size ca. 15 μm. All the chemicals were used as obtained.

A simple, surfactant-free and cost-effective solvothermal method was used to fabricate CeO$_2$ and G/CeO$_2$. The reaction took place in the beakers first and then it was shifted to an autoclave. Initially 8.642 g Ce (NO$_3$)$_3$.6H$_2$O and 11.52 g C$_6$H$_8$O$_7$ were dispersed in 100 ml distilled water separately in two beakers. These two solutions were mixed. This solution with pH 1 was stirred magnetically. A 5 M aqueous NaOH solution was then added drop-wise to the precursor solution to adjust its pH to 2. This solution was then shifted to an autoclave, which was heat-treated at 90 ℃ for 24 h. The solid was retained after washing it for three times in a centrifuge machine using distilled water and ethanol. The precipitates so collected were dried in oven at 120 ℃ overnight and were ground. The powder was heat-treated in a box furnace at 400 ℃ for 3 h to get a phase pure form.

Preparation of G/CeO$_2$ nanocomposites

Two different samples of nanocomposites were synthesized using different quantities of graphene, i.e., 12% and 25% using a similar method depicted above, except the addition of GNPs. GNPs were dispersed ultrasonically in a solution containing distilled water and isopropyl alcohol (equal volume). This solution was then added to the CeO$_2$ solution followed by similar procedure as depicted above. The process is presented schematically in Fig. 1.
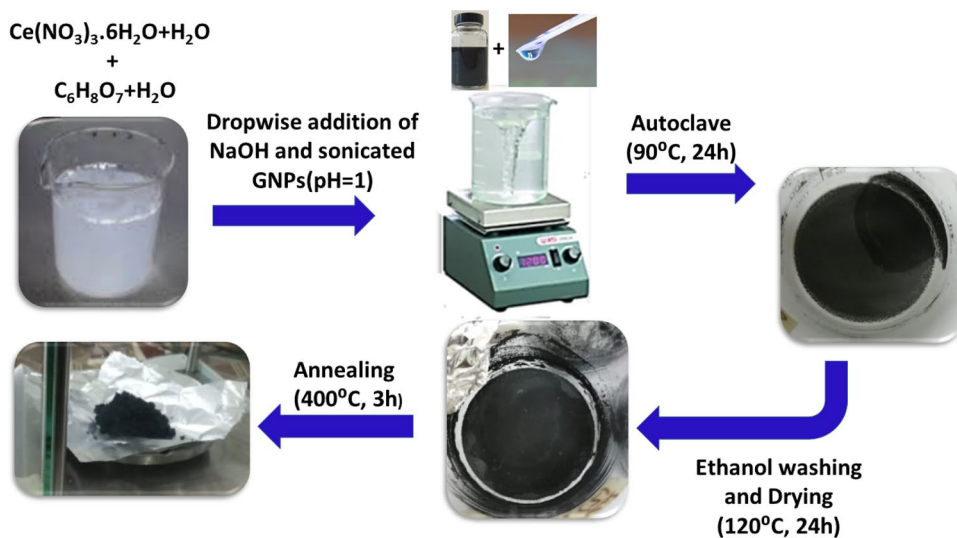
Antibacterial experiment

The effect of graphene-based CeO$_2$ nanocomposites on *P. aeruginosa* and *S. aureus* can be studied by making disc diffusion assays. Disc diffusion method or Kirby–Bauer test method is used to check the effect of antibiotics on bacteria. We have followed the same protocol as described in previous work (Luc 2015; Arshad et al. 2017a). Briefly, in this testing method, bacteria are kept in agar plates and antibiotic wafers are placed on them. 10 mg/L of each test sample (CeO$_2$, G/CeO$_2$-I and G/CeO$_2$-II) are sonicated in sterile water. 5 mL of LB medium (Luria–Bertani Broth) is mixed with 200 μL of each sonicated solution which is then inoculated into 100 μL of the bacterial culture in LB and incubated at 37 °C for 24 h.

Characterizations

The structural and phase analysis was performed using powder X-ray diffraction technique at PANalytical X'Pert PRO diffractometer. The surface, substructure and shape of prepared nanomaterials were obtained using SEM (MIRA3-TESCAN) that has a coupled electron dispersive X-ray (EDX) spectrometer. The absorbance profiles were studied using UV-1700 UV–visible spectrophotometer (SHIMADZU PharmaSpec). The Raman spectra were obtained using Raman spectrophotometer (Nost).

Fig. 1 Schematic presentation of G/CeO$_2$ synthesis

Ce(NO$_3$)$_3$.6H$_2$O+H$_2$O
+
C$_6$H$_8$O$_7$+H$_2$O

Dropwise addition of NaOH and sonicated GNPs(pH=1)

Autoclave (90°C, 24h)

Ethanol washing and Drying (120°C, 24h)

Annealing (400°C, 3h)

Results and discussion

Phase analysis

The phase purity of the samples is examined by X-ray diffraction. The XRD results of CeO_2, G/CeO_2-I and G/CeO_2-II are shown in Fig. 2. The XRD peaks of prepared samples have been obtained from 20° to 80°. Results show that CeO_2 nanotiles can be indexed to the pure fluorite cubic structure with a lattice constant $a = 5.41$ Å. These results match well with JCPDS card no. 00-004-0593 and literature (Kannan and Sundrarajan 2014; Hirano and Kato 1999). Diffraction peaks at 28.55°, 33.07°, 47.49°, 56.328°, 76.73° and 79.079° can be assigned to (111), (200), (220), (311), (331) and (420) planes of CeO_2 respectively. No impurity peaks are observed in the pure CeO_2 sample. In G/CeO_2-I and G/CeO_2-II, presence of (002) carbon peak at $2\theta = 26.228°$ proves the composition of graphene with CeO_2. This confirms the formation of biphasic G/CeO_2 nanocomposites. We have also determined the interlayer spacing of neat GNPs and G/CeO_2 nanocomposites. The interlayer spacing for neat GNPs is 3.35 Å, whereas it has increased for G/CeO_2 nanocomposites to 3.37 Å. This increase in interlayer spacing may be attributed to the presence of CeO_2 along with multiple graphene sheets. The average crystallite size is calculated using Scherrer's equation, $D = \frac{k\lambda}{\beta\cos\theta}$. The crystallite size of neat CeO_2 sample is estimated to be 14.14 nm which is reduced to 13.57 nm and 2.16 nm for G/CeO_2-I and G/CeO_2-II, as determined using (111) peak only.

Morphological study

The morphology of prepared samples has been studied by scanning electron microscope (SEM). Figure 3a–c shows the morphology details of all the three samples. Figure 3a reveals that the CeO_2 sample has nano-tiles like structure with the thickness ranging from 76 to 113 nm. Figure 3b, c depict SEM micrographs of G/CeO_2-I and G/CeO_2-II respectively. Graphene nanopatches plastered on CeO_2 nanotiles can be seen clearly, that confirm the formation of

bi-phase G/CeO_2 nanocomposites. The TEM images of G/CeO_2-II nanocomposite are presented in Fig. 3d–f. These images depict the transparent sheet-like structures are graphene sheets as observed in Fig. 3d, e. The images also show the random presence of CeO_2 nanotiles on the graphene sheets. The semi-transparent to transparent graphene nanosheets are clearly visible in Fig. 3e. Figure 3f shows that the thickness of one of the CeO_2 nanotiles is 144.4 nm. The TEM images provide further insight into the morphology of the prepared samples and confirm the formation of G/CeO_2 nanocomposite.

EDX analysis

The energy-dispersive X-ray spectroscopy has been used to investigate the elemental composition of the synthesized samples. Figure 4a shows the elemental composition of CeO_2 nanotiles. The elemental presence of Ce and O ensures the formation of CeO_2, and no impurity elements are observed. Carbon peaks can be observed in G/CeO_2-I and G/CeO_2-II nanocomposite samples, in addition to Ce and O peaks, shown in Fig. 4b, c which are due to presence of graphene. However, making the sample's surface conductive is important, which has been achieved by carbon coating on the sample's surface. Therefore, a low intensity peak related to carbon has also been observed in neat CeO_2, which is due to carbon coating. No impurity peaks have been observed.

Optical analysis

The absorbance of prepared samples is investigated using UV–vis spectrophotometer. Figure 5 shows the absorbance spectra of CeO_2 and its composites with graphene. Since, all the samples show a definite absorption peak, therefore, in this case, it is preferred to find the bandgap energies using the relation, $E_g = \left(\frac{1240}{\lambda}\right)$ eV. Here λ is the wavelength associated with the prominent peak in respective absorbance profiles of all the three samples. The bandgap energies so obtained are 4.14 eV (for CeO_2), 3.86 eV (for G/CeO_2-I) and 3.80 eV (for G/CeO_2-II). The observed bandgap of CeO_2 is

Fig. 2 **a** XRD pattern of CeO_2 and G/CeO_2 nanocomposites, and **b** C(002) peak of graphene nanoplatelets
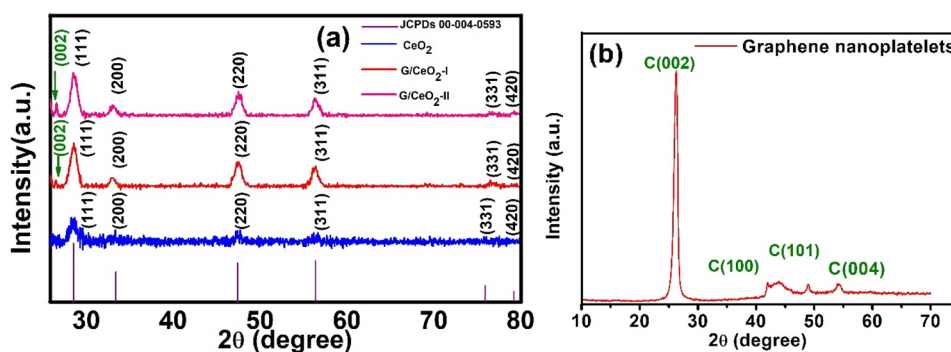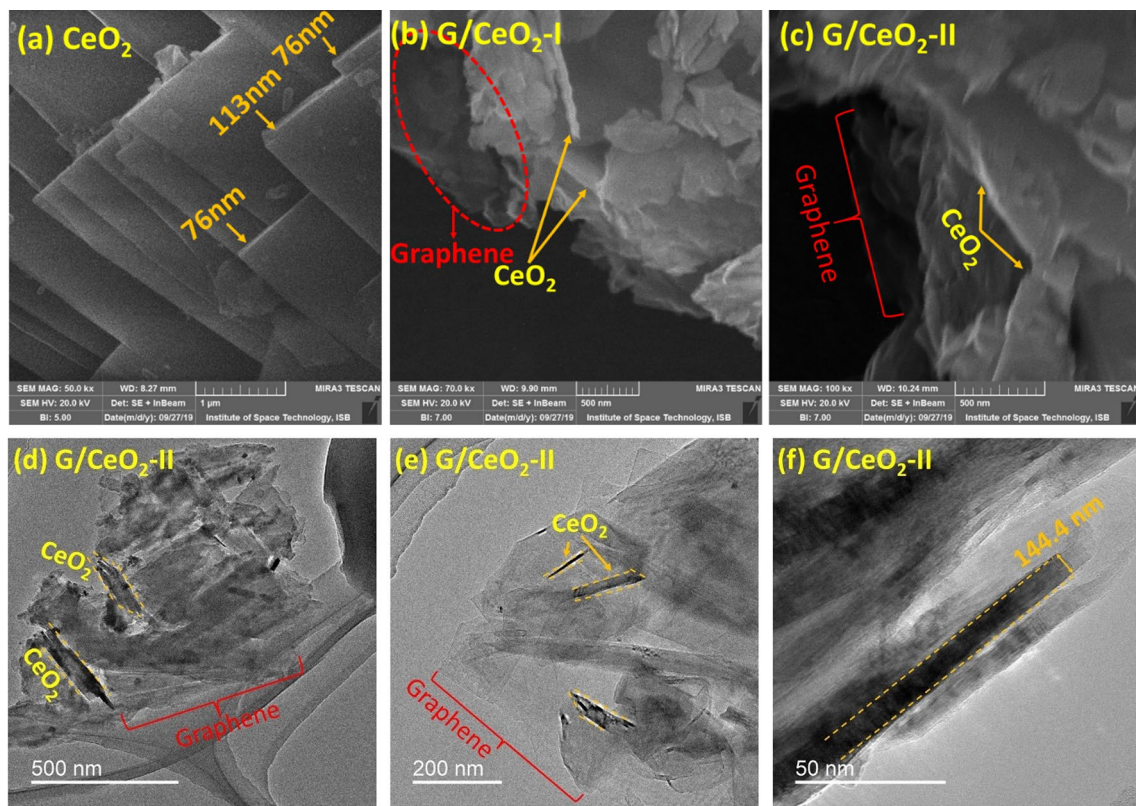
Fig. 3 SEM images of **a** CeO$_2$ nanotiles, **b** G/CeO$_2$-I, **c** G/CeO$_2$-II nanocomposites and TEM images of G/CeO$_2$-II nanocomposite **d**–**f**

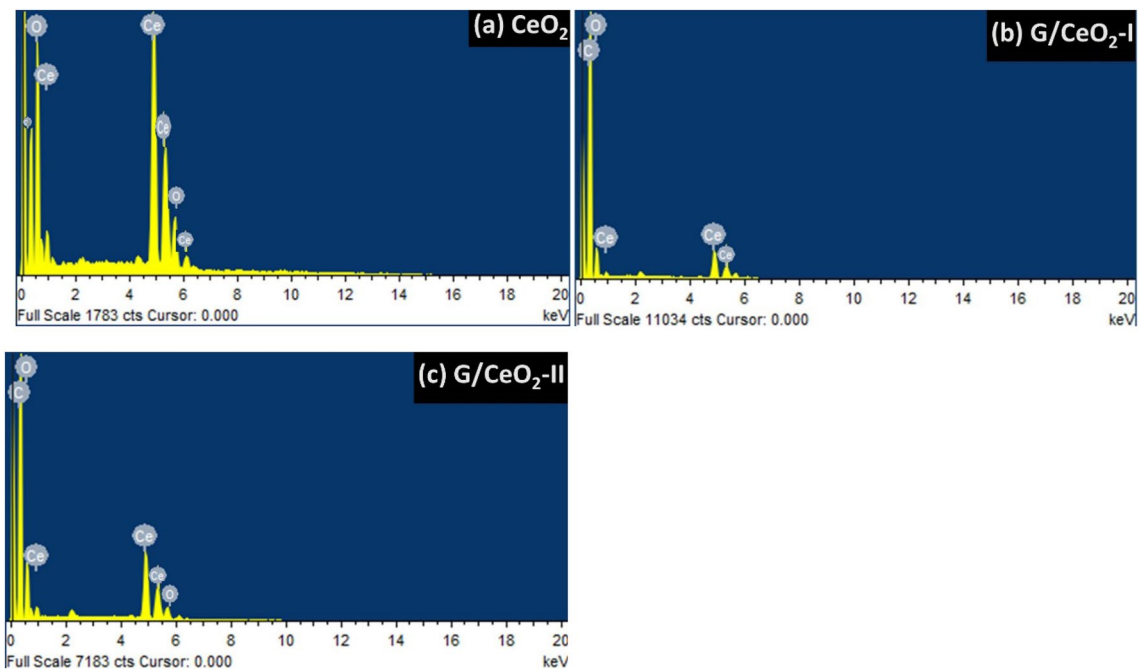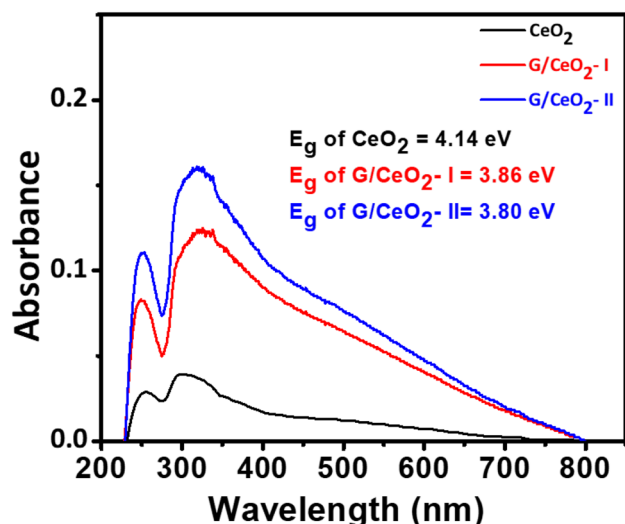**Fig. 4** EDX results of CeO$_2$ and G/CeO$_2$ nanocomposites

Fig. 5 Absorbance verses wavelength plots of CeO$_2$, G/CeO$_2$-I and G/CeO$_2$-II nanocomposites

slightly higher than the reported values for bulk CeO$_2$, but it agrees well with a study where 4.65 eV bandgap has been reported for CeO$_2$ nanoparticles (Safat et al. 2021). The quantum size effects that occur in materials with nanoscale dimension lead to an increase in bandgap energies, observed in this case (Srdanov et al. 1994). It has been observed that the bandgap energies show a decreasing trend in their value due to the inclusion of graphene, in G/CeO$_2$-I and G/CeO$_2$-II nanocomposites, respectively.

The decreasing trend of energy bandgap values is attributed to new energy levels. The existence of new energy levels between valence and conduction bands of CeO$_2$ in the nanocomposite systems are due to the modification in the electronic band structure in the composite material. Electronic interaction between CeO$_2$ and graphene sheets may result in the introduction of energy states associated with defects, and modification of band structure due to inclusion of graphene in the vicinity of CeO$_2$ (Arshad et al. 2017b).

Raman spectroscopy

The study of phonon modes of G/CeO$_2$ nanocomposite using Raman spectroscopy is presented in Fig. 6. The symmetric stretching mode of Ce–O vibrations (Fluorite, F_{2g}) is observed at 461.39 cm^{-1}. The three primary features of the graphene Raman spectra are D, D' and G band. The G peak in G/CeO$_2$-II nanocomposite is associated with E_{2g} vibrational mode of ordered in-plane sp^2 carbons and is a characteristic for all sp^2-hybridized carbon structures. The structural defects and impurities express themselves as D band. GNPs and CeO$_2$ nanotiles in the nanocomposite give rise to D band with enhanced intensity, as compared to that of neat
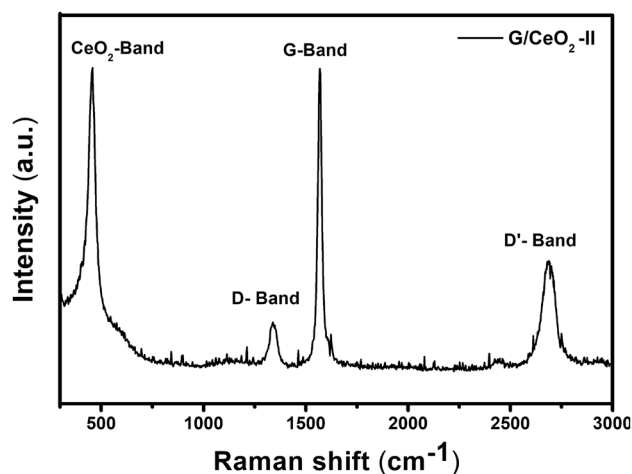

Fig. 6 Raman spectrum of G/CeO$_2$-II nanocomposite

GNPs. This also confirms the formation of nanocomposite and the surface modification of neat GNPs in the G/CeO$_2$ nanocomposite. The increased width of D band also quantifies the induced disorder in GNPs which is due to CeO$_2$ presence in the nanocomposite. The D and D' peaks exhibit themselves at 1342 cm^{-1} and 2695 cm^{-1}, respectively in G/CeO$_2$-II nanocomposite.

Antibacterial properties

The time kill assay is used to study the effect of CeO$_2$ and G/CeO$_2$ nanocomposites on Gram-negative and Gram-positive bacterial strains. The growth inhibition curves are obtained by recording optical density at 600 nm, at different intervals of time during incubation period 24 h. The control sample presents untreated bacterial strains. The bacterial growth inhibition curves of *S. aureus* and *P. aeruginosa* are shown in Fig. 7a, c, whereas Fig. 7b, d depicts the respective cell viabilities. It can be observed from antibacterial experiment that the bacterial growth is significantly inhibited in the presence of prepared materials. For *P. aeruginosa*, the growth inhibition rates are 14.21%, 61.58% and 82.67% for CeO$_2$, G/CeO$_2$-I nanocomposite and G/CeO$_2$-II nanocomposite, respectively. The growth of *S. aureus* has been controlled up to 39.53% by CeO$_2$, whereas G/CeO$_2$-I and G/CeO$_2$-II have inhibited the bacterial growth up to 62.4% and 89.48% respectively. It can be concluded from experimental data that neat CeO$_2$ nanotiles have decreased the cell growth to some extent, but the inclusion of GNPs in the nanocomposites further decreases the number of viable bacterial cells. The nanocomposite with a maximum GNPs content has achieved maximum bacterial growth inhibition rate. It is also evident that the prepared materials show selective cytotoxicity towards the Gram-negative and Gram-positive bacteria.

Fig. 7 **a** Growth profile of *P. aeruginosa* in the presence of CeO$_2$ and G/CeO$_2$ composites, **b** cell viability of *P. aeruginosa*, **c** growth profile of *S. aureus* in the presence of CeO$_2$ and G/CeO$_2$ composites and **d** cell viability of *S. aureus*
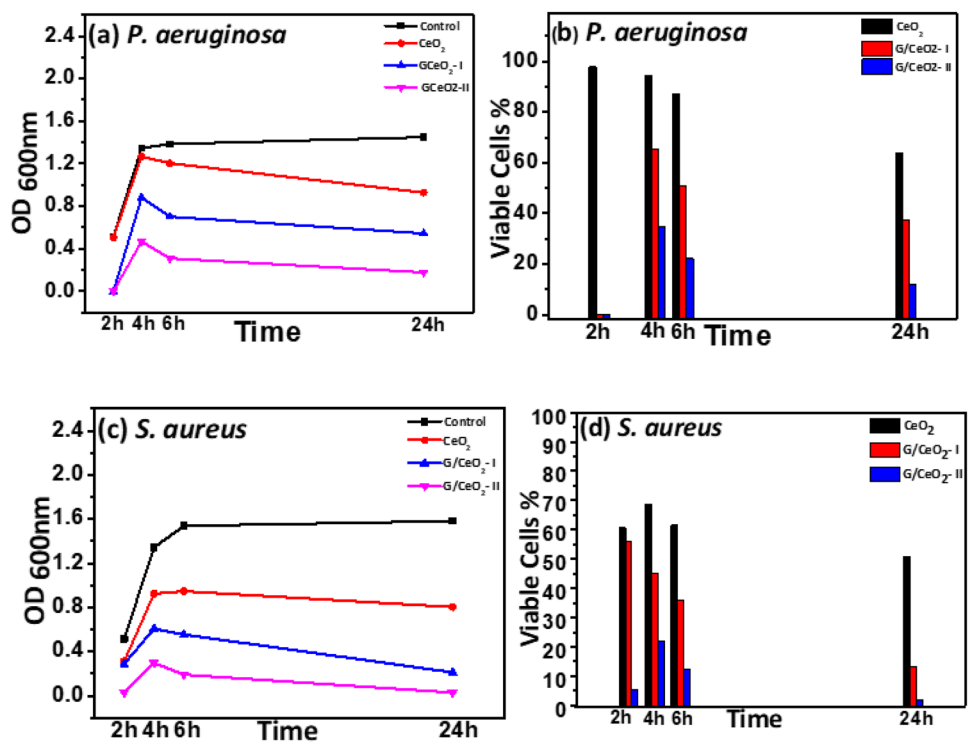
The exact mechanism for the antibacterial activity of metal oxides and graphene-based systems is still controversial; however, several hypothetical mechanisms have been proposed to account for the control of bacterial growth (Ji et al. 2016; Hegab et al. 2016). The cell composition of bacteria plays a substantial role to determine the toxicity level of prepared materials. Gram-positive bacteria have a single membrane encased by a thick peptidoglycan layer with attached proteins and different glycol polymers like polysaccharides, whereas in Gram-negative bacterial cell, the cytoplasmic membrane is covered by a thin peptidoglycan layer which is over-layered by an asymmetrical phospholipids bilayer having some polysaccharides and proteins (Shahriari et al. 2018). This difference accounts for the difference in functioning of active nanomedicine on *P. aeruginosa* and *S. aureus* as observed in the results depicted above. *S. aureus* being Gram-positive is easily targeted by G/CeO$_2$ nanocomposite as compared to *P. aeruginosa* which is Gram-negative (Arshad et al. 2017a). The selective cytotoxicity is due to different outer layers of Gram-negative and Gram-positive bacteria, as discussed above, and observed in this study.
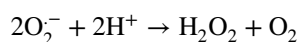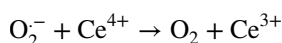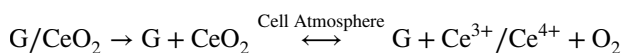
The interfusion of planar graphene on bacteria can be one of factors that is responsible for inducing the irreversible annihilation of bacterial membrane. It can be speculated form the morphology (Fig. 3) that the rough sharp edges of planar graphene exert stress on bacterial cell membrane which can cause damage to bacterial cell membrane and leakage of cytoplasmic content (Arshad et al. 2019). This disruption of membrane is not only limited to the graphene,

but the unique morphology of CeO$_2$, prepared in this work, also contributes towards bacterial membrane rupture. CeO$_2$ nanotiles enter the bacterial cell by rupturing its membrane. The sharp blade like sides of CeO$_2$ nanotiles make it easy to break the cell membranes, thus directly allowing the nanomedicine to interact with the bacterial cytoplasm. This dissolution of bacterial membrane proves to be fatal for bacteria. Also, when bacteria are exposed to CeO$_2$ nanotiles, the electrostatic charge attraction between negatively charged bacterial cell membrane and positively charged CeO$_2$ nanotiles causes its adhesion to the bacteria (Kuang et al. 2011). Moreover, graphene being an excellent electron acceptor creates a charge imbalance on the cell membrane of bacteria (Harris et al. 2010). The bacterial cell membrane and cell wall are typically negatively charged. The contact between graphene and bacterial membrane causes charge flow from membrane to the graphene conducting sheets. This charge imbalance leads to an interruption in bacterial respiratory activity that can cause bacterial cell death. The charge variation at bacterial surface may induce ROS production. The study of graphene toxicity reveals that graphene-based materials mediate oxidative stress. When cellular components are in direct contact with graphene sheets, superoxide anions are generated due to conducting graphene bridge. A related case is depicted for metallic SWCNTs, where the electron transfer from bacterial intracellular components to external environment takes place through metallic SWCNTs (Vecitis et al. 2010). Graphene can also produce similar effects by modifying bacterial DNA, lipids, and proteins by following the

similar analogy. Strong oxidation by RGO is also observed in a study (Liu et al. 2011) which also supports that rGO nanosheets can oxidize thiol groups of proteins and other bacterial cellular components.

The unique composition of prepared nanocomposites is also an important factor that determines the bacterial death. CeO_2 has a very important feature related to Ce^{3+} to Ce^{4+} ratio. CeO_2 nanotiles when enter inside bacterial cell may allow redox conversion of Ce ions. Ce^{4+} atoms may undergo a reduction process from Ce^{4+} to Ce^{3+} and vice versa in the cell environment. Generally, Ce^{3+} to Ce^{4+} ratio is maintained by $CeO_2(IV) + e^- \longrightarrow CeO_2(III)$. The ratio of Ce^{3+} also affects the bandgap values which ultimately influence the antioxidant ability of CeO_2. This transformation to Ce^{3+} is the key parameter to control the ROS generation for effective antibacterial activity (Ansari et al. 2014).

Generally, the metal oxide nanostructures (CeO_2 nanotiles, in this case) can affect the cell viability into two ways either by influencing nutrient transport or by inducing oxidative stress. NPs have a high tendency to interact with biomolecules at sub-cellular level. There are proteins present on the cell membrane that extrude from bacterial membrane to perform nutrients transportation. Ce^{4+} nanotiles bind with thiol group (-SH) of these proteins resulting in enlarged proteins and decreased membrane permeability. This leads to the bacterial cell death due to lacking nutrients (Zhang et al. 2019). The Ce^{4+} nanotiles interacting with periplasm and DNA may cause difficulty in cell respiration and interferes with DNA replication and cell division, which in turn hinders the normal function of bacteria. The other factor, i.e., oxidative stress is mainly being developed by ROS generation. ROS are generated as by product of normal metabolic reaction and mitochondrion is the leading organelle responsible for its production. While generating ATP, various ROS like free radicals (i.e., OH^-, $\cdot OH$, $^1O_2$), superoxide ions (i.e., O_2^-) and nonradical molecules (i.e., H_2O_2) are formed. Also, the inter-conversion of Ce^{3+} and Ce^{4+} amplifies ROS generation. ROS-induced bacterial cell death is composed of oxidative stress and membrane lipid peroxidation. These highly reactive oxygen species can harm the individual bacterial components, such as proteins, mitochondria and nucleic acids, which leads to the interruption of bacterial cell cycle and ultimately induces cell death (Stankic et al. 2016). A detailed version of reactions taking place between G/CeO_2 and bacteria is demonstrated below (Korsvik et al. 2007; Banavar et al. 2021):

$$G/CeO_2 \rightarrow G + CeO_2 \overset{Cell\ Atmosphere}{\longleftrightarrow} G + Ce^{3+}/Ce^{4+} + O_2$$

$$O_2^- + Ce^{4+} \rightarrow O_2 + Ce^{3+}$$

$$O_2^- + Ce^{3+} + 2H^+ \rightarrow H_2O_2 + Ce^{4+}$$

$$2O_2^- + 2H^+ \rightarrow H_2O_2 + O_2$$

Another factor that may govern the antibacterial activity is the optical bandgap energy of CeO_2. The suitable light with energy enough to generate the charge carriers (i.e., electrons and holes) when falls on the material, helps the electrons and holes to be available for the generation of ROS. The ROS are essential for effective antibacterial activity. The observed bandgap for CeO_2, and G/CeO_2 nanocomposites falls in the UV range. Therefore, only a small fraction of light photons may contribute towards the generation of reactive oxygen species, in this case. From the above discussion, we conclude that both graphene and the CeO_2 nanotiles, synergistically restrict the bacterial proliferation. A hypothetical mechanism based on the toxicity of planar graphene sheets and CeO_2 nanotiles against bacterial pathogens is shown in the Fig. 8. All the possible factors that may influence the bacterial cell death in the presence of G/CeO_2 are presented schematically below.

Various metal nanoparticles, metal oxide nanoparticles and their graphene-based composites have been employed to control bacterial growth. Biosynthesized CeO_2 NPs and their nanocomposites have been previously demonstrated as good antibacterial agents. Also, some graphene family materials have also shown significant antibacterial properties. These results are tabulated in Table 1. CeO_2 and GO/CeO_2 have been analysed as an antibacterial material previously (Bharathi and Stalin 2019; Kannan and Sundrarajan 2014; Arunachalam et al. 2018; Surendra and Roopan 2016; Hassan et al. 2012; Magdalane et al. 2017; Ravishankar et al. 2015; Yadav et al. 2017; Arumugam et al. 2015; Babu et al. 2014; Khadar et al. 2019; Wang et al. 2013; Moongraksathum and Chen 2018), but this work, for the first time evaluates the antibacterial activity of G/CeO_2 nanocomposites. The results are promising. Almost 83% growth inhibition of *P. aeruginosa* and 89% growth inhibition of *S. aureus* by the G/CeO_2 has been achieved in this work. The unique morphology of CeO_2 nanotiles has been one of the helpful factors towards achieving an excellent antibacterial performance as demonstrated in our work.

The work suggests G/CeO_2 as an effective antibacterial material. However, the performance of this material can be further investigated by studying a dose-dependent response of the prepared material. This study only addresses the use of 10 mg/L of prepared samples, which has achieved 83% and 89% growth inhibition. The work can be extended to get the response of prepared materials towards growth inhibition of other bacterial strains (not included in this work).

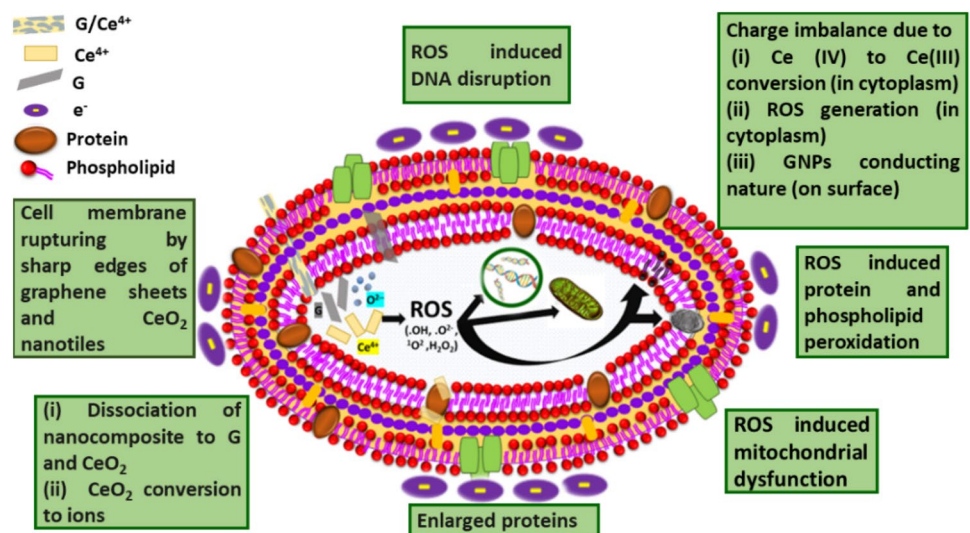**Fig. 8** Schematic illustration of antibacterial activity by G/CeO$_2$ nanocomposite

Table 1 Bacterial growth inhibition performance of different metal, metal oxide and graphene-based nanomaterials on *P. aeruginosa* and *S. aureus*

Material	Bacterial growth inhibition % or ZoI (mm) P. aeruginosa	Bacterial growth inhibition % or ZoI (mm) S. aureus	References
GO	48%	93.7%	Sengupta et al. (2019)
G QDs	Not tested	92%	Ristic et al. (2014)
CuO	Not tested	16 mm	Abboud et al. (2014)
RGO-Cu$_2$O	Not tested	65%	Yang et al. (2019)
Nitrogen doped CeO$_2$	Not tested	18 mm	Iqbal et al. (2020)
CeO$_2$ NPs extracted from Prosopis juliflora leaf	4.09 ± 0.22	12.43 ± 0.36	Arunachalam et al. (2018)
CeO$_2$ NPs extracted from Moringa oleifera peel	Not tested	5 mm	Surendra and Roopan (2016)
CeO$_2$ NPs extracted from Acalypha indicia	Not tested	90%	Kannan and Sundrarajan (2014)
Ce$_2$O$_3$/TiO$_2$	Not tested	100%	Hassan et al. (2012)
CeO$_2$/Y$_2$O$_3$	17 mm	20 mm	Magdalane et al. (2017)
CeO$_2$ NPs extracted from *Gloriosa Superba* leaf	4.50 ± 0.29	Not tested	Ravishankar et al. (2015)
CeO$_2$	Not tested	11.67 ± 0.33	Yadav et al. (2017)
CeO$_2$ NPs	4.67 mm	Not tested	Arumugam et al. (2015)
CeO$_2$/Au	Not tested	70.6%	Babu et al. (2014)
CeO$_2$-peppermint oil-PEO/GO	Not tested	22.5 mm	Bharathi and Stalin (2019)
8 M% Co doped CeO$_2$	Not tested	23 mm	Khadar et al. (2019)
Dextran coated CeO$_2$ NPs	55.4%	Not tested	Wang et al. (2013)
Ag/CeO$_2$–TiO$_2$	Not tested	99.99%	Moongraksathum and Chen (2018)
CeO$_2$ nanoparticle-coated silk fabric	65%	88%	Lu et al. (2014)
G/Cr$_2$O$_3$	80.76%	84.25%	Talat et al. (2020)
G/CeO$_2$	83%	89%	Present study

Conclusion

G/CeO$_2$ nanocomposites are successfully synthesized using a hydrothermal process. The XRD results reveal that CeO$_2$ exists as fluorite crystal structure in G/CeO$_2$ nanocomposite, thus confirming the bi-phase nature of the prepared nanocomposites. The morphology analysis obtained using FE-SEM shows that CeO$_2$ exists as nanotiles, while semi-transparent sheets like graphene are also clearly observed in the nanocomposites. The EDX results confirm the purity and elemental composition of the samples. The optical properties as obtained from UV–vis spectroscopy indicate that the

inclusion of graphene into neat CeO$_2$ decreases the bandgap up to 3.80 eV in G/CeO$_2$-II nanocomposite. The G/CeO$_2$-II nanocomposite shows excellent antibacterial activity, i.e. up to 83% loss of *P. aeruginosa* and approximately 89% in case of *S. aureus*. The antibacterial performances of all the prepared nanomaterials reveal that G/CeO$_2$-II can be considered as promising antibacterial material. It is noteworthy that the antibacterial activity of these nanomaterials may be attributed to the reversible conversion of Ce (III) and Ce (IV). The unique cutter-like morphology of CeO$_2$ and graphene inclusion synergistically enhances the activity. These findings can be a landmark to combat ADR and developing PPE (personal protective equipment) in current global health crisis.

Declarations

References

Abboud Y, Saffaj T, Chagraoui A, El Bouari A, Brouzi K, Tanane O, Ihssane B (2014) Biosynthesis, characterization and antimicrobial activity of copper oxide nanoparticles (CONPs) produced using brown alga extract (Bifurcaria bifurcata). Appl Nanosci 4:571–576

Alhazmi HA, Ahsan W, Mangla B, Javed S, Hassan MZ, Asmari M, Al Bratty M, Najmi A (2022) Graphene-based biosensors for disease theranostics: development, applications, and recent advancements. Nanotechnol Rev 11:96–116

AL-Saadi ZN, (2016) Estimation of minimum inhibitory concentration (MIC) and minimum bactericidal concentration (MBC) of cell-free extracts of bifidobacterium species against methicillin-resistant *Staphylococcus aureus* in vitro. Am J Biomed Life Sci 4:75–80

AlSheikh HMA, Sultan I, Kumar V, Rather IA, Al-Sheikh H, Tasleem Jan A, Haq QMR (2020) Plant-based phytochemicals as possible alternative to antibiotics in combating bacterial drug resistance. Antibiotics 9:480

Ansari S, Khan M, Ansari M, Lee J, Cho M (2016) Band gap engineering of CeO$_2$ Nanostructure by electrochemically active biofilm for visible light applications. RSC Adv 4:16782–16791

Arshad A, Iqbal J, Mansoor Q, Ahmed I (2017a) Graphene/SiO$_2$ nanocomposites: the enhancement of photocatalytic and biomedical activity of SiO$_2$ nanoparticles by graphene. J Appl Phys 121:244901

Arshad A, Iqbal J, Siddiq M, Mansoor Q, Ismail M, Mehmood F, Ajmal M, Abid Z (2017b) Graphene nanoplatelets induced tailoring in photocatalytic activity and antibacterial characteristics of MgO/graphene nanoplatelets nanocomposites. J Appl Phys 121:024901

Arshad A, Iqbal J, Mansoor Q (2019) Graphene/Fe3O4 nanocomposite: solar light driven Fenton like reaction for decontamination of water and inhibition of bacterial growth. Appl Surf Sci 474:57–65

Arumugam A, Karthikeyan C, Hameed ASH, Gopinath K, Gowri S, Karthika V (2015) Synthesis of cerium oxide nanoparticles using *Gloriosa superba* L. leaf extract and their structural, optical and antibacterial properties. Mater Sci Eng C 49:408–415

Arunachalam T, Karpagasundaram M, Rajarathinam N (2018) Ultrasound assisted green synthesis of cerium oxide nanoparticles using Prosopis juliflora leaf extract and their structural, optical and antibacterial properties. Mater Sci-Pol 35:791–798

Babu KS, Anandkumar M, Tsai T, Kao T, Inbaraj BS, Chen B (2014) Cytotoxicity and antibacterial activity of gold-supported cerium oxide nanoparticles. Int J Nanomed 9:5515

Banavar S, Deshpande A, Sur S, Andreescu S (2021) Ceria nanoparticle theranostics: harnessing antioxidant properties in biomedicine and beyond. J Phys Mater 4:042003

Bellio P, Luzi C, Mancini A, Cracchiolo S, Passacantando M, Di Pietro L, Perilli M, Amicosante G, Santucci S, Celenza G (2018) Cerium oxide nanoparticles as potential antibiotic adjuvant: effects of CeO$_2$ nanoparticles on bacterial outer membrane permeability. Biochimica et Biophysica Acta (BBA) Biomembranes 1860: 2428–2435

Bharathi BS, Stalin T (2019) Cerium oxide and peppermint oil loaded polyethylene oxide/graphene oxide electrospun nanofibrous mats as antibacterial wound dressings. Mater Today Commun 21:100664

Gliga AR, Edoff K, Caputo F, Källman T, Blom H, Karlsson HL, Ghibelli L, Traversa E, Ceccatelli S, Fadeel B (2017) Cerium oxide nanoparticles inhibit differentiation of neural stem cells. Sci Rep 7:1–20

Halder A, Sun Y (2019) Biocompatible propulsion for biomedical micro/nano robotics. Biosens Bioelectron 139:111334

Harris HW, El-Naggar MY, Bretschger O, Ward MJ, Romine MF, Obraztsova A, Nealson KH (2010) Electrokinesis is a microbial behavior that requires extracellular electron transport. Proc Natl Acad Sci 107:326–331

Hassan MS, Amna T, Al-Deyab SS, Kim H-C, Oh T-H, Khil M-S (2012) Toxicity of Ce$_2$O$_3$/TiO$_2$ composite nanofibers against S. aureus and S. typhimurium: a novel electrospun material for disinfection of food pathogens. Coll Surf A Physicochem Eng Aspects 415:268–273

He X, Aker WG, Huang M-J, Watts JD, Hwang H-M (2015) Metal oxide nanomaterials in nanomedicine: applications in photodynamic therapy and potential toxicity. Curr Top Med Chem 15:1887–1900

Hegab HM, ElMekawy A, Zou L, Mulcahy D, Saint CP, Ginic-Markovic M (2016) The controversial antibacterial activity of graphene-based materials. Carbon 105:362–376

Hibbitts A, Lucía A, Serrano-Sevilla I, De Matteis L, McArthur M, De La Fuente JM, Aínsa JA, Navarro F (2019) Co-delivery of free vancomycin and transcription factor decoy-nanostructured lipid carriers can enhance inhibition of methicillin resistant *Staphylococcus aureus* (MRSA). PLoS ONE 14:e0220684

Hirano M, Kato E (1999) Hydrothermal synthesis of nanocrystalline cerium (IV) oxide powders. J Am Ceram Soc 82:786–788

Huang S-H, Chen D-H (2009) Rapid removal of heavy metal cations and anions from aqueous solutions by an amino-functionalized magnetic nano-adsorbent. J Hazard Mater 163:174–179

Iqbal J, Shah NS, Sayed M, Khan JA, Muhammad N, Khan ZUH, Naseem M, Howari FM, Nazzal Y, Niazi NK (2020) Synthesis of nitrogen-doped ceria nanoparticles in deep eutectic solvent for the degradation of sulfamethaxazole under solar irradiation and

additional antibacterial activities. Chem Eng J. https://doi.org/10.1016/j.cej.2020.124869

Ji H, Sun H, Qu X (2016) Antibacterial applications of graphene-based nanomaterials: recent achievements and challenges. Adv Drug Deliv Rev 105:176–189

Jones N, Ray B, Ranjit KT, Manna AC (2008) Antibacterial activity of ZnO nanoparticle suspensions on a broad spectrum of microorganisms. FEMS Microbiol Lett 279:71–76

Joung D, Singh V, Park S, Schulte A, Seal S, Khondaker SI (2011) Anchoring ceria nanoparticles on reduced graphene oxide and their electronic transport properties. J Phys Chem C 115:24494–24500

Kannan S, Sundrarajan M (2014) A green approach for the synthesis of a cerium oxide nanoparticle: characterization and antibacterial activity. Int J Nanosci 13:1450018

Kashinath L, Namratha K, Byrappa K (2019) Microwave mediated synthesis and characterization of CeO$_2$-GO hybrid composite for removal of chromium ions and its antibacterial efficiency. J Environ Sci 76:65–79

Khadar YS, Balamurugan A, Devarajan V, Subramanian R, Kumar SD (2019) Synthesis, characterization and antibacterial activity of cobalt doped cerium oxide (CeO$_2$: Co) nanoparticles by using hydrothermal method. J Market Res 8:267–274

Kim Y, Lee W, Jung D-R, Kim J, Nam S, Kim H, Park B (2010) Optical and electronic properties of post-annealed ZnO: Al thin films. Appl Phys Lett 96:171902

Korsvik C, Patil S, Seal S, Self WT (2007) Superoxide dismutase mimetic properties exhibited by vacancy engineered ceria nanoparticles. Chem Commun. https://doi.org/10.1039/b615134e

Kuang Y, He X, Zhang Z, Li Y, Zhang H, Ma Y, Wu Z, Chai Z (2011) Comparison study on the antibacterial activity of nano-or bulk-cerium oxide. J Nanosci Nanotechnol 11:4103–4108

Kummer J (1986) Use of noble metals in automobile exhaust catalysts. J Phys Chem 90:4747–4752

Langford BJ, So M, Raybardhan S, Leung V, Westwood D, MacFadden DR, Soucy J-PR, Daneman N (2020) Bacterial co-infection and secondary infection in patients with COVID-19: a living rapid review and meta-analysis. Clin Microbiol Infect 26(12):1622–1629

Liu S, Zeng TH, Hofmann M, Burcombe E, Wei J, Jiang R, Kong J, Chen Y (2011) Antibacterial activity of graphite, graphite oxide, graphene oxide, and reduced graphene oxide: membrane and oxidative stress. ACS Nano 5:6971–6980

Lu Z, Mao C, Meng M, Liu S, Tian Y, Yu L, Sun B, Li CM (2014) Fabrication of CeO$_2$ nanoparticle-modified silk for UV protection and antibacterial applications. J Coll Interface Sci 435:8–14

Luc M (2015) A comparison of disc diffusion and microbroth dilution methods for the detection of antibiotic resistant subpopulations in Gram negative bacilli

Magdalane CM, Kaviyarasu K, Vijaya JJ, Siddhardha B, Jeyaraj B (2017) Facile synthesis of heterostructured cerium oxide/yttrium oxide nanocomposite in UV light induced photocatalytic degradation and catalytic reduction: synergistic effect of antimicrobial studies. J Photochem Photobiol B 173:23–34

Majumder MAA, Singh K, Hilaire MG-S, Rahman S, Sa B, Haque M (2020) Tackling antimicrobial resistance by promoting antimicrobial stewardship in medical and allied health professional curricula. Expert Rev Anti Infective Therapy 18:1–14

Mathew T, Sree RA, Aishwarya S, Kounaina K, Patil AG, Satapathy P, Hudeda SP, More SS, Muthucheliyan K, Kumar TN, Raghu AV, Reddy KR, Zameer F (2020) Graphene-based functional nanomaterials for biomedical and bioanalysis applications. Flat Chem 23:100184

Meixner H, Gerblinger J, Lampe U, Fleischer M (1995) Thin-film gas sensors based on semiconducting metal oxides. Sens Actu B Chem 23:119–125

Moongraksathum B, Chen Y-W (2018) Anatase TiO$_2$ co-doped with silver and ceria for antibacterial application. Catal Today 310:68–74

Ni Z, Bu H, Zou M, Yi H, Bi K, Chen Y (2010) Anisotropic mechanical properties of graphene sheets from molecular dynamics. Physica B 405:1301–1306

Paul D, Mangla S, Neogi S (2020) Antibacterial study of CuO-NiO-ZnO trimetallic oxide nanoparticle. Mater Lett 271:127740

Ravishankar TN, Ramakrishnappa T, Nagaraju G, Rajanaika H (2015) Synthesis and characterization of CeO$_2$ nanoparticles via solution combustion method for photocatalytic and antibacterial activity studies. Chem Open 4:146–154

Ristic BZ, Milenkovic MM, Dakic IR, Todorovic-Markovic BM, Milosavljevic MS, Budimir MD, Paunovic VG, Dramicanin MD, Markovic ZM, Trajkovic VS (2014) Photodynamic antibacterial effect of graphene quantum dots. Biomaterials 35:4428–4435

Rojas-Andrade MD, Chata G, Rouholiman D, Liu J, Saltikov C, Chen S (2017) Antibacterial mechanisms of graphene-based composite nanomaterials. Nanoscale 9:994–1006

Safat S, Buazar F, Albukhaty S, Matroodi S (2021) Enhanced sunlight photocatalytic activity and biosafety of marine-driven synthesized cerium oxide nanoparticles. Sci Rep 11:14734

Sanpo N, Berndt CC, Wen C, Wang J (2013) Transition metal-substituted cobalt ferrite nanoparticles for biomedical applications. Acta Biomater 9:5830–5837

Sengupta I, Bhattacharya P, Talukdar M, Neogi S, Pal SK, Chakraborty S (2019) Bactericidal effect of graphene oxide and reduced graphene oxide: influence of shape of bacteria, Colloid and Interface Science. Communications 28:60–68

Shahriari S, Monajjemi M, Zare K (2018) Increasing the efficiency of some antibiotics on penetrating bacteria cell membrane, Ukrainian. J Ecol 8:671–679

Srdanov VI, Blake NP, Markgraber D, Metiu H, Stucky GD (1994) Alkali metal and semiconductor clusters in zeolites. In: Jansen JC, Stöcker M, Karge HG, Weitkamp J (eds) Studies in surface science and catalysis. Elsevier, Amsterdam, pp 115–144

Stankic S, Suman S, Haque F, Vidic J (2016) Pure and multi metal oxide nanoparticles: synthesis, antibacterial and cytotoxic properties. J Nanobiotechnol 14:1–20

Stoianov O, Ivanov V, Shcherbakov A, Stoyanova I, Chivireva N, Antonovich V (2014) Determination of cerium (III) and cerium (IV) in nanodisperse ceria by chemical methods. Russ J Inorg Chem 59:15–23

Subbiahdoss G, Sharifi S, Grijpma DW, Laurent S, van der Mei HC, Mahmoudi M, Busscher HJ (2012) Magnetic targeting of surface-modified superparamagnetic iron oxide nanoparticles yields antibacterial efficacy against biofilms of gentamicin-resistant staphylococci. Acta Biomater 8:2047–2055

Surendra T, Roopan SM (2016) Photocatalytic and antibacterial properties of phytosynthesized CeO$_2$ NPs using Moringa oleifera peel extract. J Photochem Photobiol B 161:122–128

Talat I, Arshad A, Mansoor Q (2020) Graphene nanoplatelets/Cr$_2$O$_3$ nanocomposites as novel nanoantibiotics: towards control of multiple drug resistant bacteria. Ceram Int 47(1):889–898

Todar K (2006) Todar's online textbook of bacteriology. University of Wisconsin-Madison Department of Bacteriology Madison, Wis, USA

Tong SY, Davis JS, Eichenberger E, Holland TL, Fowler VG (2015) Staphylococcus aureus infections: epidemiology, pathophysiology, clinical manifestations, and management. Clin Microbiol Rev 28:603–661

Vecitis CD, Zodrow KR, Kang S, Elimelech M (2010) Electronic-structure-dependent bacterial cytotoxicity of single-walled carbon nanotubes. ACS Nano 4:5471–5479

Wang Z, Lee Y-H, Wu B, Horst A, Kang Y, Tang YJ, Chen D-R (2010) Anti-microbial activities of aerosolized transition metal oxide nanoparticles. Chemosphere 80:525–529

Wang G, Bai J, Wang Y, Ren Z, Bai J (2011) Prepartion and electrochemical performance of a cerium oxide–graphene nanocomposite as the anode material of a lithium ion battery. Scripta Mater 65:339–342

Wang Q, Perez JM, Webster TJ (2013) Inhibited growth of Pseudomonas aeruginosa by dextran-and polyacrylic acid-coated ceria nanoparticles. Int J Nanomed 8:3395

Wu Y, Shu R, Zhang J, Wan Z, Shi J, Liu Y, Zhao G, Zheng M (2020) Oxygen vacancies regulated microwave absorption properties of reduced graphene oxide/multi-walled carbon nanotubes/cerium oxide ternary nanocomposite. J Alloys Compd 819:152944

Xie A, Tao F, Li T, Wang L, Chen S, Luo S, Yao C (2018) Graphene-cerium oxide/porous polyaniline composite as a novel electrode material for supercapacitor. Electrochim Acta 261:314–322

Yadav LR, Lingaraju K, Prasad BD, Kavitha C, Banuprakash G, Nagaraju G (2017) Synthesis of CeO_2 nanoparticles: photocatalytic and antibacterial activities. Eur Phys J plus 132:239

Yang X, Ouyang Y, Wu F, Hu Y, Zhang H, Wu Z (2016) In situ & controlled preparation of platinum nanoparticles dopping into graphene sheets@ cerium oxide nanocomposites sensitized screen printed electrode for nonenzymatic electrochemical sensing of hydrogen peroxide. J Electroanal Chem 777:85–91

Yang X, Ouyang Y, Wu F, Hu Y, Ji Y, Wu Z (2017) Size controllable preparation of gold nanoparticles loading on graphene sheets@ cerium oxide nanocomposites modified gold electrode for non-enzymatic hydrogen peroxide detection. Sens Actu B Chem 238:40–47

Yang Z, Hao X, Chen S, Ma Z, Wang W, Wang C, Yue L, Sun H, Shao Q, Murugadoss V (2019) Long-term antibacterial stable reduced graphene oxide nanocomposites loaded with cuprous oxide nanoparticles. J Coll Interface Sci 533:13–23

Zhang M, Yuan R, Chai Y, Wang C, Wu X (2013) Cerium oxide–graphene as the matrix for cholesterol sensor. Anal Biochem 436:69–74

Zhang M, Zhang C, Zhai X, Luo F, Du Y, Yan C (2019) Antibacterial mechanism and activity of cerium oxide nanoparticles. Sci China Materi 11:1–13

Zhang J, Ding E, Xu S, Li Z, Fakhri A, Gupta VK (2020) Production of metal oxides nanoparticles based on poly-alanine/chitosan/reduced graphene oxide for photocatalysis degradation, anti-pathogenic bacterial and antioxidant studies. Int J Biol Macromol 164:1584–1591